The Numerical Modeling of Surface Wave Propagation in the Surf Zone

B. JOHNS AND R. J. JEFFERSON

Department of Meteorology, University of Reading, Reading, England

(Manuscript received 15 November 1979, in final form 31 March 1980)

ABSTRACT

A numerical model is used to simulate the shoreward propagation of a train of periodic borelike surface disturbances in the surf zone over a sloping beach. Turbulence production is included both in the shear layer at the beach and at the face of each breaking wave, and the numerical solution is used to evaluate the relative importance of these two processes. The bottom stress is calculated and the variation of this during a wave cycle is related to the form of the surface profile. Calculations also are made of the velocity profile during a wave cycle in the shear layer adjacent to the beach and the representation of this is considered in terms of a constant stress layer logarithmic profile.

1. Introduction

The propagation of breaking waves through the surf zone is relevant to coastal processes such as beach formation and the development of longshore currents. A numerical model describing the propagation of a turbulent shallow-water borelike disturbance toward a shoreline has been given by Johns (1980). This model is characterized by the use of an equation for the turbulent energy density in the system and incorporates source terms simulating turbulence production both in the shear layer adjacent to the beach and also at the face of a breaking wave. This procedure follows closely the methods applied in the analysis of the turbulent shear-wave boundary layer beneath regular sinusoidal surface waves (Johns, 1977) and the calculation of the turbulent tidal flow in an elongated channel (Johns, 1978). The model was used to investigate the dynamical structure beneath both a single bore and a periodic sequence of bores entering the analysis region from the open sea. Conclusions were drawn concerning the bottom friction, its relationship to the borelike propagation and the effectiveness of an empirically based quadratic law to represent the bottom stress.

The present paper forms a continuation and development of the earlier work. Using as a basis the model given by Johns (1980), we have prescribed that a train of periodic disturbances enter the surf zone from the open sea. As these move toward the shoreline, they soon steepen and assume the form of propagating bores in which there is a generation of turbulent energy both in the shear layer adjacent to the beach and at the face of each wave. We have used the solution to estimate the contribution to the turbulent energy budget made by turbulence production at the face of a wave and, compared with the shear layer production, have shown that this effect is predominant in determining the attenuation of the waves as they approach the shoreline.

Our solution is used to calculate the friction velocity at the beach and the variation of this during a wave cycle is compared with that of the depth-averaged velocity between the free surface and the beach. We find that these velocities are approximately in phase during the wave cycle and this suggests that a useful empirically based relation may exist between the two. Equivalently, we have determined a friction coefficient in a quadratic friction law and have related this to the wave period and bottom roughness.

Finally, we have investigated the Reynolds-averaged velocity structure in the shear layer adjacent to the beach in which the bulk of the velocity variation occurs. A typical thickness of this layer is determined and the velocity profiles, computed at a sequence of instants during the wave cycle, show features observed in experimental studies of turbulent boundary layers beneath waves. We also find an offshore time-averaged current which tends to balance the onshore time-averaged volume flux of water resulting from the mass transport associated with the primary wave. An examination of these velocity profiles leads to the possibility of representing them in terms of a constant stress layer logarithmic profile. We investigate the effectiveness of this procedure for varying bottom roughness conditions and find that the goodness of the resulting approximation is a function of the roughness length of the bottom elements. An explanation of this result is not easy to find but it

0022-3670/80/071061-09$06.25

does suggest that some caution is required in using a constant stress hypothesis as a basis for the indirect determination of the bottom stress beneath waves.

2. Formulation

A Cartesian frame of reference is used in which Ox is normal to the shoreline and which is fixed in the equilibrium level of the free surface. The origin O is located at the seaward extremity of the analysis region and Oz points vertically upward. The equilibrium position of the shoreline is at $x = L$ and the equilibrium depth of the water over a plane sloping beach is given by

$$h(x) = h_0\left(1 - \frac{x}{L}\right), \tag{2.1}$$

where h_0 is the undisturbed depth at $x = 0$.

The development of a set of equations describing the propagation of a shallow water turbulent bore toward a shoreline has been given by Johns (1980). We summarize these equations here and refer to the earlier work for details of the hypotheses in the formulation. Additionally, as in Johns (1980), we transform the vertical coordinate so that the beach and free surface correspond to fixed coordinate levels. With some approximation, this procedure then yields an equation for the Reynolds-averaged velocity u given by

$$\frac{\partial u}{\partial t} + u\frac{\partial u}{\partial x} + \omega\frac{\partial u}{\partial \sigma} = -g\frac{\partial H}{\partial x} - \frac{gh_0}{L} + \frac{\partial}{\partial x}\left(N\frac{\partial u}{\partial x}\right) + \frac{1}{H^2}\frac{\partial}{\partial \sigma}\left(K\frac{\partial u}{\partial \sigma}\right). \tag{2.2}$$

In this, σ is related to z and the displacement ζ of the free surface about the equilibrium level by

$$\sigma = \frac{z + h}{H}; \tag{2.3}$$

the quantity ω is given by

$$\omega = \sigma_t + u\sigma_x + w\sigma_z. \tag{2.4}$$

H is the total depth $\zeta + h$, and N and K refer to coefficients for horizontal and vertical turbulent exchange processes, respectively.

The equation of volume continuity has the form

$$\frac{\partial H}{\partial t} + \frac{\partial}{\partial x}\left[H\int_0^1 u\,d\sigma\right] = 0 \tag{2.5}$$

and the Reynolds-averaged turbulent energy density E satisfies

$$\frac{\partial E}{\partial t} + u\frac{\partial E}{\partial x} + \omega\frac{\partial E}{\partial \sigma} = \frac{K}{H^2}\left(\frac{\partial u}{\partial \sigma}\right)^2 + N\left(\frac{\partial u}{\partial x}\right)^2 + \frac{\partial}{\partial x}\left(N\frac{\partial E}{\partial x}\right) + \frac{1}{H^2}\frac{\partial}{\partial \sigma}\left(K\frac{\partial E}{\partial \sigma}\right) - \epsilon, \tag{2.6}$$

where ϵ specifies the dissipation of turbulence energy. The vertical motion is determined diagnostically from

$$H\omega = \sigma\frac{\partial}{\partial x}\left[H\int_0^1 u\,d\sigma\right] - \frac{\partial}{\partial x}\left[\int_0^\sigma u\,d\sigma\right]. \tag{2.7}$$

In the vertical exchange terms, turbulence closure is attained by use of the relation

$$K = c^{1/4}lE^{1/2}, \tag{2.8}$$

where $c = 0.08$ and the length scale l is determined from

$$l = \frac{-\kappa(E^{1/2}/l)}{\frac{d}{dz}(E^{1/2}/l)}, \quad l = \kappa z_0 \text{ as } z \to -h. \tag{2.9}$$

The quantity κ is von Kármán's constant 0.4 and z_0 is the roughness length of the bottom elements.

The horizontal exchange coefficient is related to the turbulence energy density by

$$N = \alpha LE^{1/2}, \tag{2.10}$$

where $\alpha L(\alpha < 1)$ is a length scale associated with the horizontal mixing. The dissipation is parameterized according to

$$\epsilon = \frac{c^{3/4}E^{3/2}}{l}. \tag{2.11}$$

The accompanying boundary conditions are discussed by Johns (1980) and yield

$$\left.\begin{aligned} u &= 0 \quad \text{at} \quad \sigma = 0 \\ \omega &= 0 \quad \text{at} \quad \sigma = 0 \quad \text{and} \quad \sigma = 1 \\ \frac{\partial u}{\partial \sigma} &= 0 \quad \text{at} \quad \sigma = 1 \\ \frac{\partial E}{\partial \sigma} &= 0 \quad \text{at} \quad \sigma = 0 \quad \text{and} \quad \sigma = 1 \end{aligned}\right\}. \tag{2.12}$$

3. Solution procedure

The scaling procedure used by Johns (1980) shows that the solution of the equations in Section (2) depends on parameters z_0/h_0, α, h_0/L and on quantities describing the wave input at the seaward end of the analysis region. In the present work, we prescribe an oscillatory wave input given by

$$H = h_0 + a\sin\left(\frac{2\pi t}{t_p}\right) \quad \text{at} \quad x = 0. \tag{3.1}$$

Additionally, then, the oscillatory response in $0 < x \leq L$ depends on an amplitude factor a/h_0 and a nondimensional wave period equal to $t_p(gh_0)^{1/2}/L$.

The solution procedure is closely related to that used by Johns (1978) with the modifications given by Johns (1980) to cater for the moving shoreline.

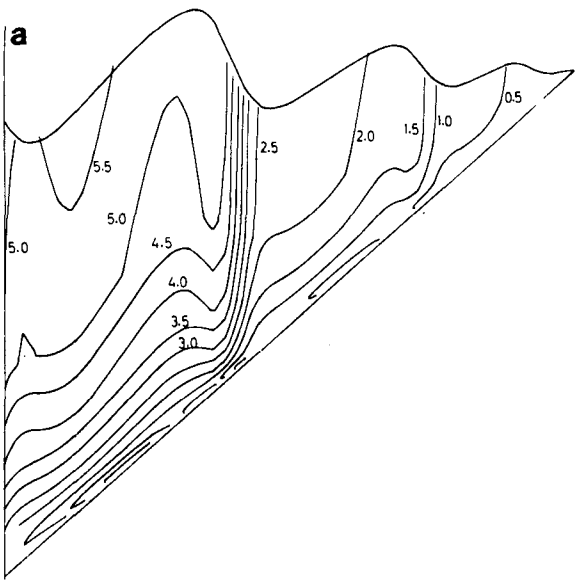

FIG. 1a. Contours of equal values of $10^3E/(gh_0)$ beneath the waves with horizontal production included at $t = 0$.

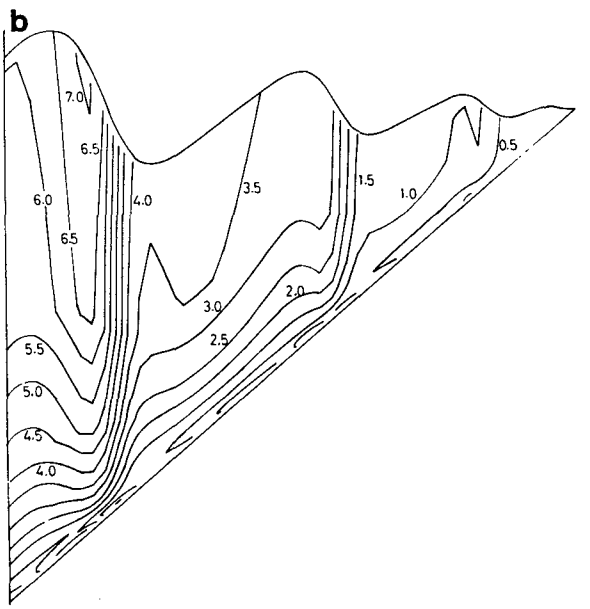

FIG. 1b. As in Fig. 1a except that $t = t_p/2$.

There are 10 unequally spaced computational levels in the vertical with a staggered grid in the horizontal having 101 points ($\Delta x = L/100$). The elevations and currents are recorded at odd and even points, respectively. The system is integrated ahead in time from an initial state of rest and the integration continued until the transients in the response are dissipated by friction thus leaving a purely oscillatory solution. This then forms the basis of the diagnostic analyses described in this paper.

4. Numerical experiments

The first experiments performed are concerned with the distribution of turbulence energy beneath the waves and, in particular, with the effect of including the horizontal production term $N(\partial u/\partial x)^2$ in (2.6). In the experiments, we take $\alpha = 0.1$, $h_0/L = 0.025$, $z_0/h_0 = 0.002$, $a/h_0 = 0.16$ and a nondimensional wave period equal to 0.5. This parameter setting, later referred to as (A), corresponds to a typical surf zone-dimensional setting in which $h_0 = 2.5$ m, $L = 100$ m, $z_0 = 5$ mm, $a = 40$ cm and $t_p = 10.1$ s.

It is appropriate at this stage to discuss the anticipated breaking characteristics of the primary wave as it propagates toward the shoreline. The local wavelength of the primary wave at $x = 0$ is $t_p(gh_0)^{1/2}$ and the ratio of the wave height and the wavelength is $2a/[t_p(gh_0)^{1/2}] \approx 0.016$. The beach slope amounts to 1/40 and the wave breaking indices given by Horikawa (1978, p. 54) suggest that the deforming incoming wave will begin to break when the local water depth to wave height ratio is ~1.7. This suggests that the position of breaking, where $x = x_b$ is given by $x_b/L = 1 - 3.4(a/h_0) \approx 0.45$. Consequently, in our numerical experiments, the seaward 45% of the analysis area is used to model the incoming wave as it steepens from its primary regular form. Over the remaining 55% of the analysis area, the wave is assumed to propagate as a shallow-water bore at the face of which turbulence production is parameterized by the term $N(\partial u/\partial x)^2$. In our formulation, it will be assumed that this turbulence production extends throughout the depth of the water (except in so far as it is affected by depth variations in N or equivalently E) and is not confined to the near-surface. A prescribed attenuation with depth could have been incorporated into the parameterization but, at this stage of the modeling procedure, the additional empirical input was not thought desirable. It will also be noted that the horizontal production term is included in that part of the propagation region seaward of the anticipated breaking zone. However, the production process is self-regulating and governed by the horizontal velocity gradients that develop beneath the deforming wave profile.

With the horizontal production included in (2.6), we give in Figs. 1a and 1b contours of equal values of $10^3E/gh_0$ at the instants $t = 0$ and $t = t_p/2$, respectively. Superimposed on these is the profile of the free surface from which the relatively steep front of each wave is apparent. Also evident as the waves approach the shoreline is the decrease in amplitude and the wave set-up that occurs.

Associated with the face of each wave, we note the effect of the horizontal production term and how this generates a tail of turbulence energy that spreads downward and backward to affect the

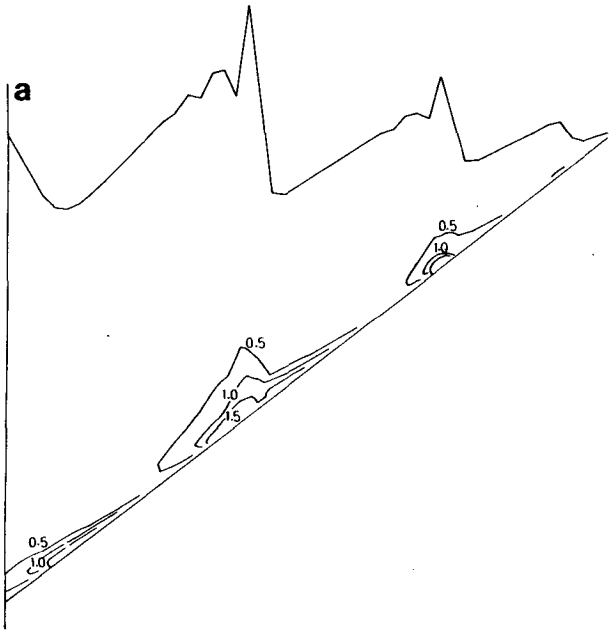

FIG. 2a. As in Fig. 1a except that horizontal production is excluded.

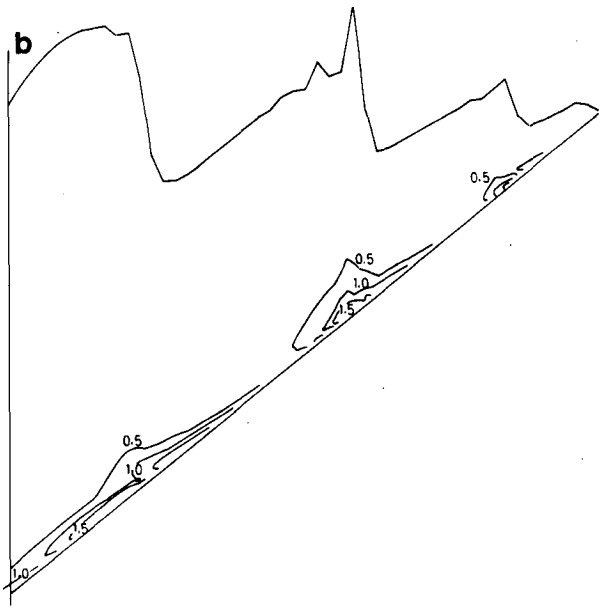

FIG. 2b. As in Fig. 1b except that horizontal production is excluded.

turbulence intensity adjacent to the sloping beach. These general effects are supported in experimental work reported by Peregrine and Svendsen (1978) who describe the development of a turbulent region behind the toe of a roller and which remains attached to the free surface. Measurements by Resch *et al.* (1976) beneath a stationary hydraulic jump also reveal this feature and tend to confirm our hypothesis of the borelike character of the disturbed free surface. Values of E/gh_0 adjacent to the beach are of order 10^{-3} and imply a turbulent velocity scale of 0.03 $(gh_0)^{1/2}$. Maximum values of E/gh_0 occur at the face of the breaking wave and can attain values of $\sim 7 \times 10^{-3}$.

In order to evaluate the full effect of the horizontal production term, it is informative to repeat the above calculations with $N(\partial u/\partial x)^2$ removed from (2.6). We still retain the horizontal mixing term in (2.2) which implies a drain of energy from the Reynolds-averaged flow. However, this energy is not then retained in the turbulence energy budget and is not therefore available to contribute to the value of the exchange coefficients in (2.8) and (2.10). In particular, the value of E in (2.10) will be reduced with a corresponding reduction in the value of N. The effect of this will be to reduce the strength of the horizontal mixing of momentum in (2.2) and therefore to lessen the smoothing of the surface profile the effect of which is apparent in Figs. 1a and 1b. That this is in fact the case may be seen from Figs. 2a and 2b. The surface profile is now sharper with steeper wave fronts. Additionally, there is evidence of subsidiary wavelets behind the crest of each of the breakers. With horizontal production included in the turbulent energy balance, the increased horizontal mixing smoothes out these subsidiary wavelets. In a sense, then, the inclusion of the horizontal production term in (2.6) is equivalent to an increase in the value of the horizontal mixing scale αL used in (2.10). However, changes in the horizontal mixing scale cannot directly influence the value of the vertical exchange coefficient and, from this point of view, the retention of the horizontal production term forms an essential part of the way in which the bottom shear layer is reproduced in the model.

Other important conclusions to be drawn from Figs. 2a and 2b relate to the distribution of contours giving equal values of $10^3E/gh_0$. Maximum values of the turbulence intensity now occur in the shear layer adjacent to the beach and a typical value of E/gh_0 is 3×10^{-3}. The increased value of E (relative to the case with horizontal production included) is a consequence of the increased value of the surface wave height resulting from the decrease in horizontal mixing and the correspondingly reduced attenuation of the waves as they progress toward the shoreline.

The contrasting results obtained in these two cases indicate the importance of retaining the energy extracted from the Reynolds-averaged flow and not viewing the process purely from the point of view of numerically treating developing discontinuities by the use of an artificial viscosity (Lax and Wendroff, 1960). They also underline the need to determine the value of α on the basis of experiment so as

to produce the correct wave attenuation in the model. On general grounds, it may in fact be anticipated that α is an increasing function of distance from the shoreline and not a constant.

The distribution of turbulence energy determined in these calculations immediately yields the bottom stress τ_b through the relation

$$\frac{\tau_b}{\rho} = c^{1/2}E_b \operatorname{sgn}\left[\left(\frac{\partial u}{\partial \sigma}\right)_{\sigma=0}\right], \tag{4.1}$$

where E_b is the turbulence energy density at $\sigma = 0$. Equivalently, the bottom friction velocity u_* is given by

$$u_* = c^{1/4}E_b^{1/2} \operatorname{sgn}\left[\left(\frac{\partial u}{\partial \sigma}\right)_{\sigma=0}\right]. \tag{4.2}$$

It is informative to compare the temporal variation of u_* with that of the depth-averaged velocity $\bar{u}$ given by

$$\bar{u} = \int_0^1 u d\sigma. \tag{4.3}$$

With the parameter setting (A), and with horizontal production included, we give (in Fig. 3) the temporal variation of $u_*/(gh_0)^{1/2}$ and $\bar{u}/(gh_0)^{1/2}$ during a wave cycle at a position P at $x = 59\Delta x$.

It is noteworthy that the sense of the friction velocity changes abruptly during the wave cycle. These changes precede the time of reversal in the sense of the depth-averaged velocity by approximately $(0.05)t_p$ and imply that the sense of the bottom stress changes almost discontinuously during the wave cycle. This result is a consequence of the use of a gradient transfer law for vertical momentum exchanges and may, perhaps, be indicative of the need for a higher order turbulent closure scheme. Our computed results imply that the change in sense occurs in a time of order $(0.01)t_p$. Although this has been adequately resolved in our numerical time-stepping procedure, a corresponding instrumentational resolution would be difficult to achieve in an attempt at experimental verification.

In spite of the above comments, the variation of the bottom friction velocity is seen to be approximately in phase with that of the depth-averaged velocity and this suggests that it may be worthwhile to consider an approximate representation of the bottom stress in terms of a bottom friction law of the form

$$\frac{\tau_b}{\rho} = C_f \bar{u}|\bar{u}|. \tag{4.4}$$

As in Johns (1977), the friction coefficient is given by

$$C_f = u_*^2/\bar{u}^2 \tag{4.5}$$

and, in general, this will have a temporal variation

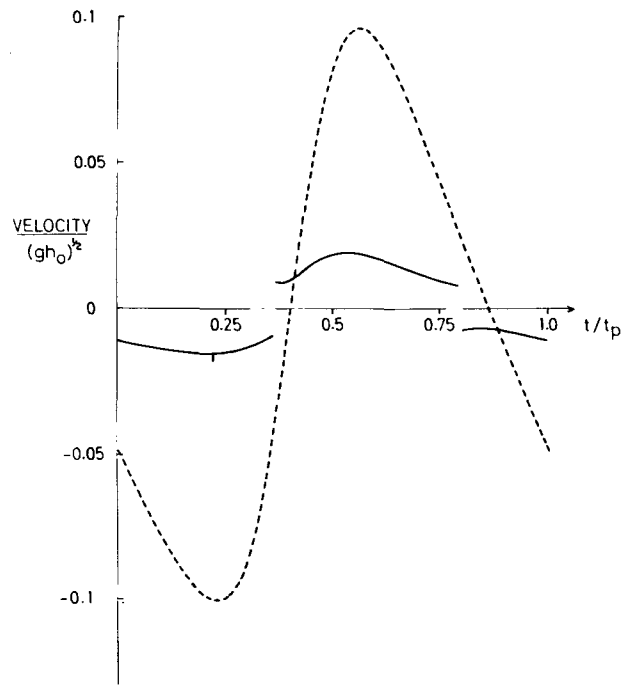

FIG. 3. Variation of $u_*/(gh_0)^{1/2}$ and $\bar{u}/(gh_0)^{1/2}$ at $x = 59\Delta x$ during a wave cycle. The continuous line is the friction velocity, the broken line is the depth-averaged velocity.

during the wave cycle. However, an optimized and temporally invariant form may be defined by

$$C_f = \frac{\int_0^{t_p} (\bar{u}u_*)|\bar{u}u_*|dt}{\int_0^{t_p} \bar{u}^4 dt}. \tag{4.6}$$

With a friction coefficient given by (4.6), it is then possible to compare the representation (4.4) with (4.1) evaluated from our numerical model. In Fig. 4 we give the variation of $10^3\tau_b/\rho g h_0$ during a wave cycle as computed from (4.1) and (4.4) at position P.

We note that the quadratic friction law underestimates the magnitude of the onshore bottom stress and overestimates the magnitude of the offshore bottom stress. In relation to the peak values of the stress, these under- and overestimates are, respectively, of order 19% and 35% of the model value and must be expected to give rise to a significant error if used in an assessment of the bed-load transport of bottom material. Additionally, the quadratic friction law fails to reproduce the abrupt changes in the bottom stress near the time of flow reversal.

Our calculations of C_f as given by (4.6) have been carried out with fixed values of the nondimensional wave period and roughness parameters in the parameter setting (A) and, in circumstances when the

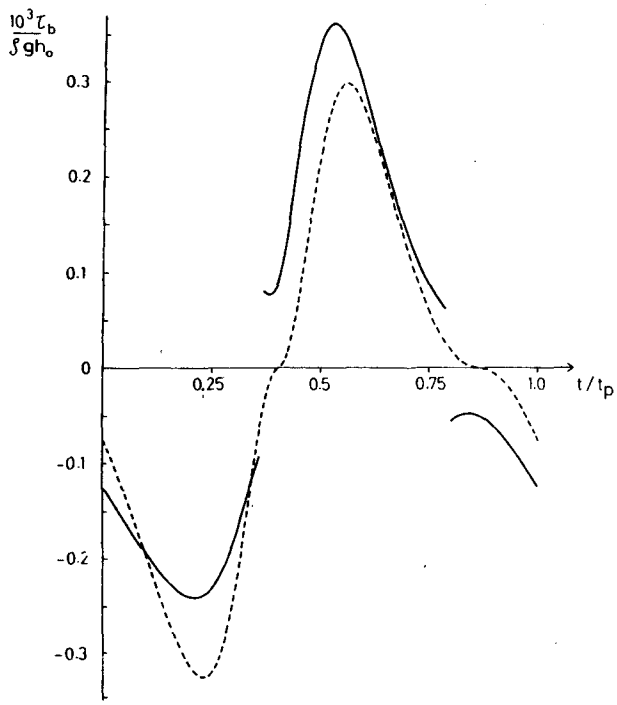

FIG. 4. Variation of $10^3\tau_b/(\rho g h_0)$ at $x = 59\Delta x$ during a wave cycle. Continuous line is from Eq. (4.1). The broken line is from Eq. (4.4) with C_f given by Eq. (4.6).

quadratic friction law might be deemed adequate, it is informative to know in what way the friction coefficient depends on these quantities. The effect of variations in the nondimensional wave period has been investigated by repeating the earlier calculations but with a systematic variation of the wave period.

Using a least-squares-fitting procedure, the results have been represented in terms of a power law having the form

$$C_f = C\left[\frac{t_p(gh_0)^{1/2}}{L}\right]^n, \tag{4.7}$$

where C and n depend on the horizontal spatial position.

We consider here four positions corresponding to $x = (i - 1)\Delta x$ with $i = 20, 40, 60, 80$. With a nondimensional wave period between 0.5 and 2.0, the corresponding values of C and n are given in Table 1. Hence, with $i = 60$ and with the extreme nondimensional periods of 0.5 and 2.0, the corresponding friction coefficients are 2.89×10^{-2} and 0.96×10^{-2}, respectively. The friction coefficient therefore reduces with an increasing value of the wave period. The reason for this is that the bottom stress is determined by the turbulence energy density. As the wave period increases, the wave input into the analysis region becomes less frequent and at a fixed position turbulence will be generated less frequently by the action of the production terms in (2.6). Consequently, in the intervening period, the background of residual turbulence persisting from one wave cycle to the next will have a longer interval of time in which to decay, thus reducing the value of the bottom stress. For a fixed input amplitude, however, the depth-averaged velocity will be of a comparable value for all wave periods. This tendency is then reflected in a reduced value of the friction coefficient. It is of some interest to note that this tendency is to be expected throughout the frequency spectrum up to the scale of tidal waves where the friction coefficient is well-documented as being of order 2.6×10^{-3}. The results in Table 1 also indicate that the friction coefficient has a significant variation over the length of the analysis region and attains a maximum near the shoreline.

TABLE 1. Values of quantities in Eq. (4.7) giving the variation of friction coefficients with the wave period.

i	20	40	60	80
C	0.0149	0.0147	0.0167	0.0233
n	−0.593	−0.896	−0.793	−0.584

TABLE 2. Values of quantities in Eq. (4.8) giving the variation of friction coefficients with the roughness length.

i	20	40	60	80
C	0.290	0.362	0.326	0.439
n	0.402	0.421	0.374	0.395

The effect of variations in the roughness parameter has been investigated in a similar way by using the parameter setting (A) and carrying out a systematic variation of z_0/h_0 for values between 0.00025 and 0.002. Again, the results have been fitted to a power-law representation having the form

$$C_f = C\left(\frac{z_0}{h_0}\right)^n \tag{4.8}$$

and values of C and n have been evaluated at spatial positions corresponding to $i = 20, 40, 60, 80$. These are given in Table 2. Hence, with $i = 60$ and with the extreme roughness parameters 0.00025 and 0.002, the corresponding friction coefficients are, respectively, 1.47×10^{-2} and 3.19×10^{-2} implying an increase in the friction coefficient with increasing bottom roughness.

In Johns (1977), an analogous representation of C_f is obtained for the boundary friction beneath progressive sinusoidal surface waves. That result shows a similar qualitative behavior of the friction

coefficient as in the present work and implies a decrease in C_f with either an increase in the wave period or a decrease in the bottom roughness.

In order to investigate the effectiveness of the quadratic friction law in representing the bottom stress in the interval $0 < x < L$, it is convenient to use the temporally invariant optimized value of C_f given in (4.6) and to apply this in (4.4) with the variation with x referred to above. The resulting bottom stress may then be compared with the model evaluation based on (4.1). Using the parameter setting (A), the results of this comparison are given in Fig. 5. In this $\tau_b/\rho g h_0$ is evaluated at the commencement of a wave cycle for the interval $0 < x < L$. The surface elevation is superimposed on the same diagram which enables the occurrence of the peak stresses to be related to the form of the surface profile. We again note that the quadratic law tends to underestimate the onshore bottom stress, especially beneath the face of a breaking wave. It is also noteworthy that the peak value of the onshore stress always occurs in front of the wave crest. Beneath the sloping back of the wave, the quadratic law representation compares well with the model value although some deviation occurs in the neighborhood of a flow reversal where an abrupt change in the sign of the model stress is again apparent. Peak values of the offshore bottom stress occur beneath the wave troughs and their magnitude tends to be overestimated by the quadratic law.

The experimental determination of the bottom stress beneath waves, especially with the instrumentational resolution required to test the results in this paper, raises difficult problems. A frequently used technique to derive the bottom stress depends on the assumption of a constant stress layer logarithmic bottom velocity profile in which

$$u = \frac{u_*}{\kappa} \ln\left(\frac{z + h + z_0}{z_0}\right). \tag{4.9}$$

By using measured values of the near bottom velocity, it is possible to fit these to a relation having the form (4.9) and then to deduce the value of $\tau_b = \rho u_* |u_*|$. This procedure has been used by Jonsson and Carlsen (1976) and its successful application clearly depends on the actual existence of a constant stress logarithmic layer.

The model described in this paper may be used to investigate the near-bottom velocity profile and to test the hypotheses used in the indirect determination of τ_b described above. We note first that our numerical model yields $\tilde{u}^2/\overline{u^2} < 1.04$ and this result, obtained also by Johns (1978, 1980), indicates an almost uniform velocity structure through the depth. The only significant variation in the velocity structure occurs in a thin shear layer adjacent to the beach and, in the present work, we concentrate on this region.

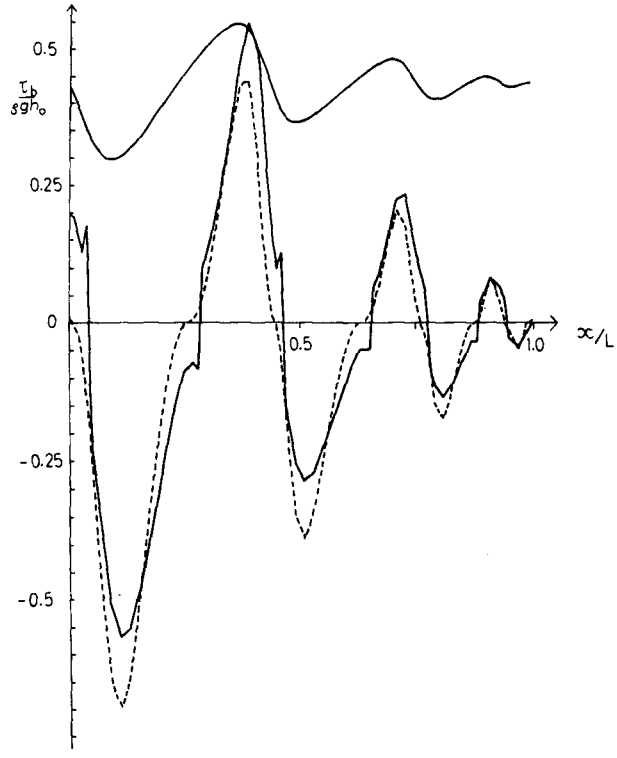

FIG. 5. Variation of $\tau_b/(\rho g h_0)$ beneath the waves at $t = 0$.

Using the parameter setting (A), we give in Fig. 6 the variation of the near bottom velocity at P at a sequence of instants during a wave cycle. Throughout the cycle, the velocity is almost uniform with depth at heights above the roughness elements in excess of $(0.15)h_0$. As may be seen, however, the bulk of the shear is confined to a layer whose thickness is of order $(0.05)h_0$. Taking $h_0 = 2.5$ m in the parameter setting (A), this corresponds to an effective shear layer thickness of ~12 cm. This compares well with measurements made in an oscillating water tunnel and reported by Jonsson (1978). We also note the characteristic overshooting of the near bottom velocities above the mid-depth value which is again observed in the experimental studies described by Jonsson (1978).

We have used the numerical solution described above to determine the time-mean properties of the velocity field during a wave cycle. Defining the time-mean of a quantity ϕ by

$$\langle \phi \rangle = \frac{1}{t_p} \int_0^{t_p} \phi \, dt, \tag{4.10}$$

we find at P, and with the parameter setting (A), that $\langle u \rangle < 0$ throughout the depth. In the mid-depths, $\langle u \rangle/(g h_0)^{1/2} \sim -0.006$ and so there is an offshore residual velocity corresponding to a return flow which compensates for the onshore mean volume flux of water generated by the mass transport

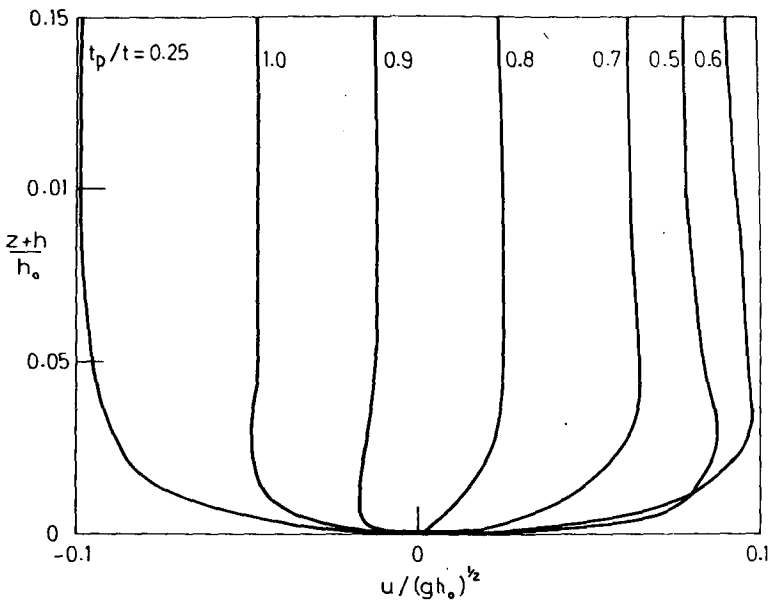

FIG. 6. Variation of the near-bottom velocity at $x = 59\Delta x$ during a wave cycle.

associated with the incoming primary wave. This acts to make the value of $\langle H \int_0^1 u d\sigma \rangle$ zero. With $h_0 = 2.5$ m, the mid-depth offshore residual current is of order 3 cm s^{-1}.

In order to evaluate the effectiveness of the constant stress hypothesis (4.9) with $|u_*| = c^{1/4}E_b^{1/2}$, we have made a comparison of (4.9) with the model profile at P at instants during the wave cycle with the parameter setting (A) but with a variation of z_0/h_0. The variation of $u/(gh_0)^{1/2}$ in the shear layer is given in Figs. 7a and 7b at two instants during the cycle for $z_0/h_0 = 0.0005$ and 0.002, respectively.

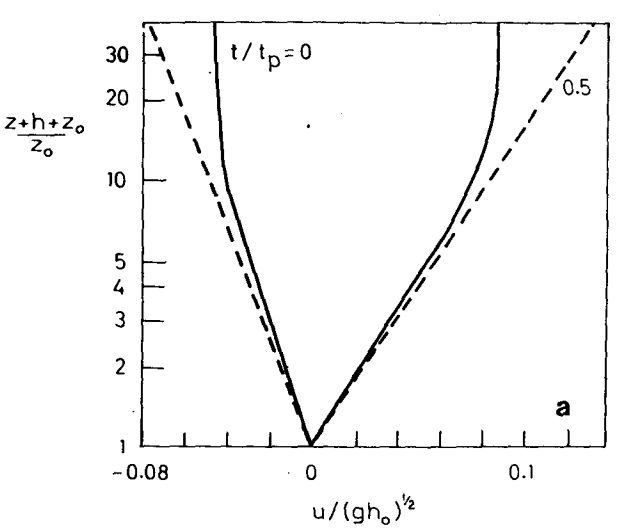

FIG. 7a. Variation of $u/(gh_0)^{1/2}$ at $x = 59\Delta x$ at $t = 0$ and $t = t_p/2$ with $z_0/h_0 = 0.0005$. The continuous line is from the model calculation, the broken line is from Eq. (4.9) with $u_* = c^{1/4}E_b^{1/2}$.

These figures indicate clearly a reduction in the shear layer thickness with an increase in z_0/h_0. They also show that the constant stress profile hypothesis becomes less tenable with a decrease in z_0/h_0. A reason as to why this should be so is not clear, but it does suggest that indirect procedures for the determination of the bottom stress beneath waves should be viewed with some caution.

It must be stated clearly that the work described in this paper is a first step toward the satisfactory modeling of surf zone processes. As has been mentioned, there are indications that the assumed gradient law for momentum transport may be deficient and that our use of the associated turbulence closure scheme in a high-frequency reversing flow situation may be questionable. We would claim, however, that the present scheme represents an advance on earlier parameterizations of fric-

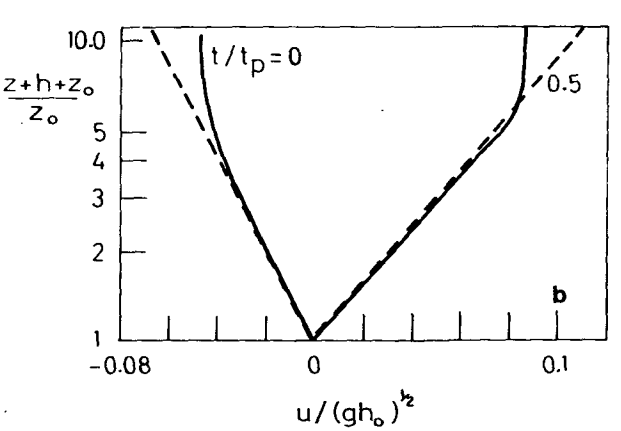

FIG. 7b. As in Fig. 7a except that $z_0/h_0 = 0.002$.

tional processes in the surf zone that depend almost entirely on heavy empirical input.

Acknowledgment. One of us (RJJ) acknowledges support as a post-doctoral research fellow by the U.K. Natural Environment Research Council during the period of this investigation.

REFERENCES

Horikawa, K., 1978: *Coastal Engineering*. University of Tokyo Press, 402 pp.

Johns, B., 1977: Residual flow and boundary shear stress in the turbulent bottom layer beneath waves. *J. Phys. Oceanogr.*, **7**, 733–738.

——, 1978: The modeling of tidal flow in a channel using a turbulence energy closure scheme. *J. Phys. Oceanogr.*, **8**, 1042–1049.

——, 1980: The modelling of the approach of bores to a shoreline. *Coastal Eng.*, **3**, 207–219.

Jonsson, I. G., 1978: A new approach to oscillatory rough boundary layers. Series Pap. 17, Institute of Hydrodynamics and Hydraulic Engineering, Technical University of Denmark, 87 pp.

——, and N. A. Carlsen, 1976: Experimental and theoretical investigations in an oscillatory rough turbulent boundary layer. *J. Hydrol. Res.*, **14**, 45–60.

Lax, P., and B. Wendroff, 1960: Systems of conservation laws. *Commun. Pure Appl. Math.*, **13**, 217–237.

Peregrine, D. H., and I. A. Svendsen, 1978: Spilling breakers, bores and hydraulic jumps. *Proc. 16th Coastal Eng. Conf.*, Hamburg, Amer. Soc. Civil Eng. and Coastal Eng. Res. Council, 1–11.

Resch, F. J., H. J. Leutheussen and M. Coantic, 1976: Étude de la structure cinématique et dynamique du ressaut hydraulique. *J. Hydraul. Res.*, **14**, 293–318.